The Astrophysical Journal, 613:312–321, 2004 September 20

SYNTHETIC LICK INDICES AND DETECTION OF α-ENHANCED STARS. II. F, G, AND K STARS IN THE $-1.0 <$ [Fe/H] $< +0.50$ RANGE

M. Franchini, C. Morossi, and P. Di Marcantonio
INAF–Osservatorio Astronomico di Trieste, Via G.B. Tiepolo, 11, I-34131 Trieste, Italy;
franchini@ts.astro.it, morossi@ts.astro.it, dimarcan@ts.astro.it

M. L. Malagnini
Dipartimento di Astronomia, Università degli Studi di Trieste, Via G.B. Tiepolo, 11, I-34131 Trieste, Italy; malagnini@ts.astro.it

and

M. Chavez and L. Rodríguez-Merino
Instituto Nacional de Astrofísica, Optica y Electrónica, A.P. 51 y 216, 72000 Puebla, Mexico; mchavez@inaoep.mx, lino@inaoep.mx
Received 2004 April 1; accepted 2004 May 28

ABSTRACT

We present an analysis of 402 F, G, and K solar neighborhood stars, with accurate estimates of [Fe/H] in the range -1.0 to $+0.5$ dex, aimed at the detection of α-enhanced stars and at the investigation of their kinematical properties. The analysis is based on the comparison of 571 sets of spectral indices in the Lick/IDS system, coming from four different observational data sets, with synthetic indices computed with solar-scaled abundances and with α-element enhancement. We use selected combinations of indices to single out α-enhanced stars without requiring previous knowledge of their main atmospheric parameters. By applying this approach to the total data set, we obtain a list of 60 bona fide α-enhanced stars and of 146 stars with solar-scaled abundances. The properties of the detected α-enhanced and solar-scaled abundance stars with respect to their [Fe/H] values and kinematics are presented. A clear kinematic distinction between solar-scaled and α-enhanced stars was found, although a one-to-one correspondence to "thin disk" and "thick disk" components cannot be supported with the present data.

Subject headings: Galaxy: stellar content — stars: abundances — stars: kinematics — stars: late-type

Online material: machine-readable table

1. INTRODUCTION

The presence of different chemical compositions in mildly metal-poor and solar galactic stars with similar [Fe/H] is widely recognized. In particular, high-resolution studies show scatters in individual element abundance ratios at different extent in different [Fe/H] ranges (see, e.g., Bensby et al. 2003 and references therein). These spreads are attributed mainly to the presence of different components in the Galaxy, in general, and in the Galactic disk, in particular (see, e.g., Norris 1999). The observed abundance patterns, together with kinematical information, can in fact be used to discriminate among different Galaxy formation and evolution interpretations (see, e.g., Nissen 2004).

Of particular relevance are the abundance and kinematical analyses of stars characterized by the so-called α-enhancement phenomenon, which gives insights into the role, for instance, of Type I and Type II supernovae in the chemical enrichment of individual stellar populations (Chen et al. 2003). Most of the analyses refer to main-sequence or slightly evolved stars of spectral types F, G, and K because their atmospheres still present the original chemical composition of their birth places.

In general, detailed high-resolution analysis of individual stars is needed to tackle the problem of determining individual element abundances. This kind of approach can be complemented by a statistical one based on lower resolution data in wavelength ranges selected for extracting absorption features representative of relevant elemental species. It is also worth noting that such an analysis is particularly suitable for interpreting the integrated light of distant stellar clusters and external galaxies. In Franchini et al. (2003, hereafter Paper I) we proposed selected combinations of Lick/IDS indices capable of singling out α-enhanced stars without requiring previous knowledge of their main atmospheric parameters. This approach was applied to the stars in the Worthey et al. (1994) catalog, leading to the detection of 82 candidate α-enhanced stars. The validity of our method was established by comparison with element abundance determinations from high-resolution spectroscopy. The purpose of this paper is to use this method to detect the α-enhanced and solar-scaled abundance (SSA) stars in a much larger observational data set by using an expanded grid of synthetic indices. We concentrate our attention on the [Fe/H] regime in which the presence of both α-enhanced and SSA stars and their relative frequency are still under investigation, i.e., $-1.0 <$ [Fe/H] $< +0.5$. The [Fe/H] distributions and the kinematical properties of the identified α-enhanced stars will then be compared in a statistical way with those of SSA stars in order to investigate if the two groups belong or not to a same Galactic component.

In §§ 2 and 3 the stellar sample and the theoretical grids and indices, respectively, are presented. The detection of stars with α-element enhancement is described in § 4. Section 5 contains a discussion on the chemical and kinematical properties of the program stars. Concluding remarks are given in § 6.

2. THE STELLAR SAMPLE

The selection of stars to be analyzed requires previous knowledge of their [Fe/H] in order to deal only with mildly

metal-poor, solar, and supersolar stars, i.e., with [Fe/H] in the range -1.0 to 0.5 dex. There are several estimates of [Fe/H] available from the literature (see, e.g., the compilation by Cayrel et al. 2001), but the lack of homogeneity limits the usability of these sources as input for our selection. Therefore, we decided to use the two [Fe/H] catalogs by Taylor (1999, 2003b), which ensure overall homogeneity of the analysis and internal consistency. These catalogs contain F, G, and K stars of luminosity classes II–V and provide not only mean values of [Fe/H] but also their rms errors. The selection in [Fe/H] provides a list (hereafter identified as TAYCAT) of 2014 stars (922 dwarfs and 1092 giants) that were searched for in different observational data sets suitable for deriving the spectral feature indices to be used in our analysis. In this paper we take into account the behavior of the four Lick/IDS indices, namely, Ca4227, Mg_2, Mg *b*, and Na D, already found relevant to the detection of α-enhanced candidate stars in Paper I.

2.1. *The Observational Data Sets*

Four observational data sets were searched for stars in common with TAYCAT: one of these, the Cananea collection, is a set of newly observed spectra, while the other three data sets, the Worthey catalog, the STELIB library, and the ELODIE archive, are from the literature. Of these, only one is a collection of indices, while the others are spectroscopic data sets. The cross-correlation of TAYCAT with these sources allow us to assemble a total sample of 402 F, G, and K stars as described below.

The Worthey catalog (Worthey et al. 1994) contains 21 Lick/IDS indices of 460 stars of different spectral types. All the F, G, and K stars in this catalog were already analyzed in Paper I. The 168 in common with TAYCAT are considered here for completeness and comparison purposes. Hereafter, the indices from this data set will be identified by the subscript W.

The other three data sets are collections of spectra taken with different instruments, and they are listed hereafter in order of increasing spectral resolution:

1. *The Cananea collection*.—A set of 400 stars, mainly G-type, was observed during two runs at the 2.12 m *f*/12 telescope of the INAOE "G. Haro" Observatory in Cananea (Mexico) with a Böller & Chivens spectrograph working at the resolution of 15 Å FWHM at 5000 Å for determination of atmospheric parameters (see Morossi et al. 2002). Each stellar frame was accompanied by a calibration spectrum of a reference He-Ar lamp, and standard stars were observed several times during each night to allow relative flux calibration. Unfortunately, seeing conditions were not exceptional, and only parts of the nights were of photometric quality, thus preventing, in several cases, the achievement of an accurate flux calibration. On the other hand, a good wavelength calibration was achieved with a typical rms uncertainty of ± 1.0 Å throughout the whole sampled stellar spectrum. Correction of stellar data for individual Doppler shift was done by fitting the barycenters of selected and easily identifiable features. The spectra have been used to measure spectral indices in the four aforementioned Lick system bands, and the 54 stars in common with Worthey et al. (1994) were used to find the transformation coefficients, via a linear regression, between the observational and the Lick/IDS systems. Figure 1 shows the agreement between the calibrated indices and the corresponding Worthey ones. It can be seen that apart from the case of few outliers (indicated by their HD number), the points cluster around the 45° line with deviations on the order of the observational errors given in Worthey et al. (1994). As for the computed indices from the Cananea collection, their uncertainties estimated from multiple observations of the same stars are comparable with the Worthey ones.

Of the total Cananea collection, 135 stars are in common with TAYCAT. Indices from multiple observations of the same star were averaged after calibration to increase their accuracy. Hereafter, the indices computed from the spectra in this data set will be identified by the subscript C.

2. *The STELIB library*.—This new spectroscopic stellar library (Le Borgne et al. 2003)[1] consists of a homogeneous library of 249 stellar spectra in the visible range 3200–9500 Å, with an intermediate spectral resolution (3 Å) and sampling (1 Å). This library includes stars of various spectral types and luminosity classes, spanning a relatively wide range in metallicity. The spectra are flux-calibrated and corrected for interstellar extinction and radial velocity. The overall absolute photometric uncertainty is 3%. The spectra have been degraded to the resolution of the Lick/IDS spectra, the four spectral indices in the Lick system bands were measured, and the 37 stars in common with Worthey et al. (1994) were used to find the transformation coefficients between the observational and the Lick/IDS systems. Figure 2 shows the agreement between the calibrated indices and the corresponding Worthey ones. It can be seen that the points cluster around the 45° line with deviations on the order of the observational errors given in Worthey et al. (1994). We assume the uncertainties affecting STELIB indices to be equal to the Worthey ones. The two outliers in the Mg *b* plot have indices quite far from the range of the other 32 stars, but they do not affect the calibration parameters. There are 73 spectra in this data set in common with TAYCAT; their computed indices will be identified by the subscript S hereafter.

3. *The ELODIE archive*.[2]—This archive contains all the data taken with the ELODIE spectrograph and makes them available through the World Wide Web in a readily usable form. ELODIE is an echelle spectrograph in use at the 1.93 m telescope of Observatoire de Haute Provence (OHP) since late 1993 (Baranne et al. 1996). The original spectra, which have a nominal resolution of $R = 42,000$, have been corrected for radial velocity and degraded to the resolution of the Lick/IDS spectra. The four spectral indices in the Lick system bands were measured, and 82 stars in common with Worthey et al. (1994) were used to find the transformation coefficients between the observational and the Lick/IDS systems. Figure 3 shows the agreement between the calibrated indices and the corresponding Worthey ones. As in the Cananea case, the uncertainties affecting the computed indices are comparable to the Worthey ones. Only the uncertainty affecting the Na D index, whose wavelength range presents several gaps in the original spectra, is, in general, slightly higher. Hereafter, the indices computed for the 195 stars in this data set in common with TAYCAT will be identified by the subscript E.

The numbers of stars in common between TAYCAT and each of the four data set are given in Table 1. The total working sample consists of 571 sets of four indices referring to a total of 402 individual stars. The list of all the stars is given in Table 2.[3] The distribution of [Fe/H] of the 402 program stars is shown in Figure 4. The giant and dwarf groups contain almost the same number of objects, 196 and 206, respectively, and do not show significant differences in their [Fe/H] distributions. In

[1] STELIB is available at http://webast.ast.obs-mip.fr/stelib.

[2] The ELODIE archive is available at http://atlas.obs-hp.fr/elodie.

[3] This table is available in its entirety in the electronic edition of the *Astrophysical Journal*.

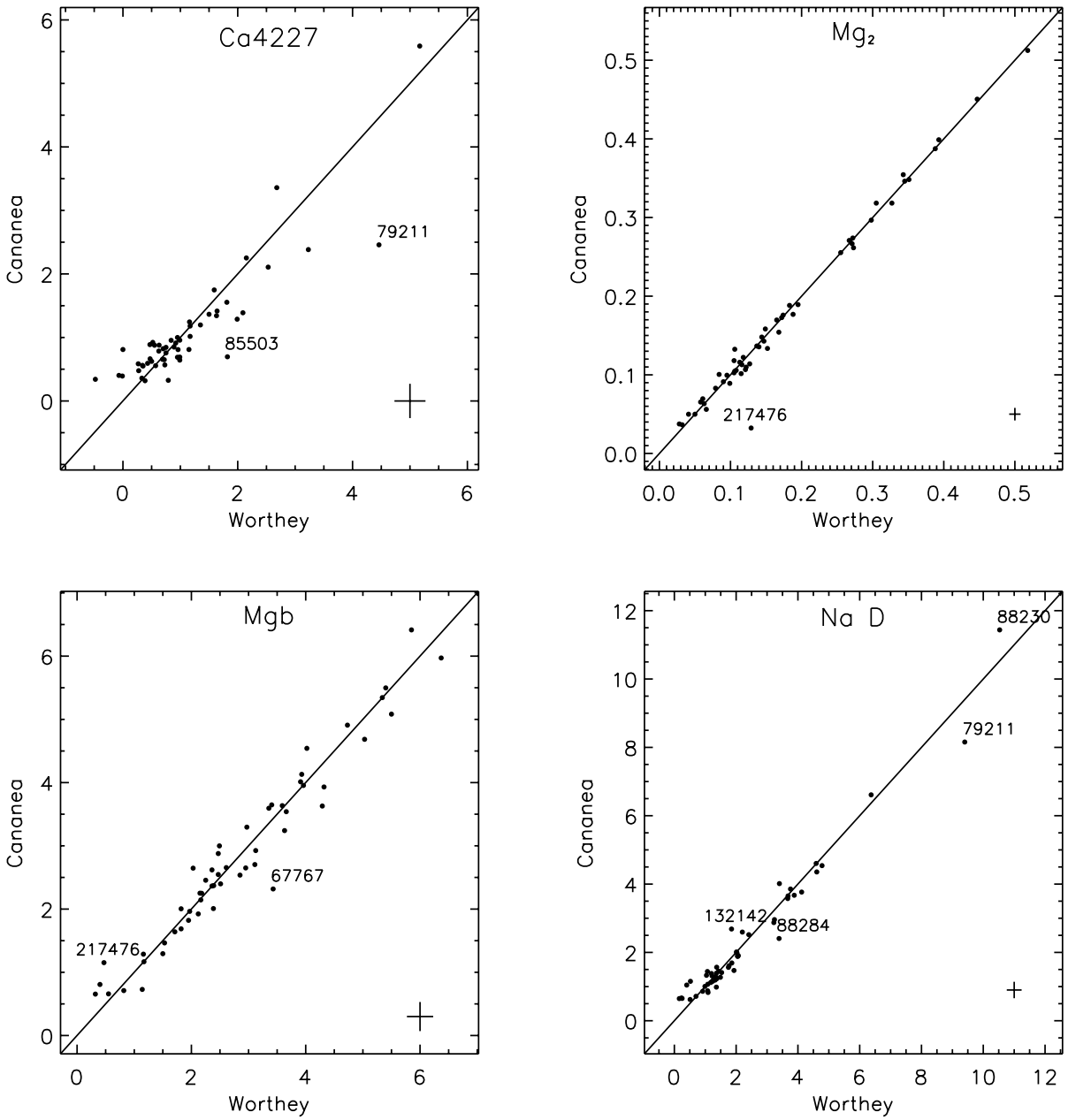

FIG. 1.—Comparison of the calibrated indices of the Cananea collection with the corresponding Worthey catalog indices. Outliers are indicated by their HD number, and observational errors are indicated by crosses in each panel.

both cases the [Fe/H] distributions are peaked around solar metallicity, with a shallow left tail extending down to $[\mathrm{Fe/H}] = -1.0$ dex.

3. SYNTHETIC SPECTRA AND INDICES

In order to have a theoretical counterpart of the observational data sets, we started from the library of 336 synthetic spectra, computed by using the stellar spectral synthesis program SPECTRUM (Gray & Corbally 1994), presented in Paper I. The library has been extended by adding two new sets at $[\mathrm{Fe/H}] = -1.5$ and $[\mathrm{Fe/H}] = -2.0$, for the α-enhanced (non-SSA [NSSA]) and SSA grids, respectively. Furthermore, the sampling in surface gravity was reduced from 1.0 to 0.5 dex, and the $\log g$ values span a wider range starting from 0.5 dex (but for the SSA grid at $[M/\mathrm{H}] = +0.5$, which is computed at $\log g = 2.0$, 3.0, 4.0, and 5.0 dex only). The final library consists of 888 synthetic spectra computed with the same characteristics described in Paper I. We recall that the SSA grid refers to SSAs, based on Grevesse & Sauval (1998) solar abundances, while the NSSA grid refers to NSSAs with enhanced α over iron ratios $[\alpha/\mathrm{Fe}] = +0.4$. The α-elements considered are O, Ne, Mg, Si, S, Ar, Ca, and Ti. It is worth noting that all the synthetic spectra were computed by using models and opacity distribution functions in a fully consistent way. The four synthetic indices Ca4227, Mg_2, Mg b, and Na D were computed and then calibrated by using the same transformation coefficients of Paper I.

4. DETECTION OF CANDIDATE α-ENHANCED STARS

The detection of α-enhanced stars by comparing the observed spectra with the ad hoc computed SSA and NSSA synthetic ones would be straightforward if we unambiguously

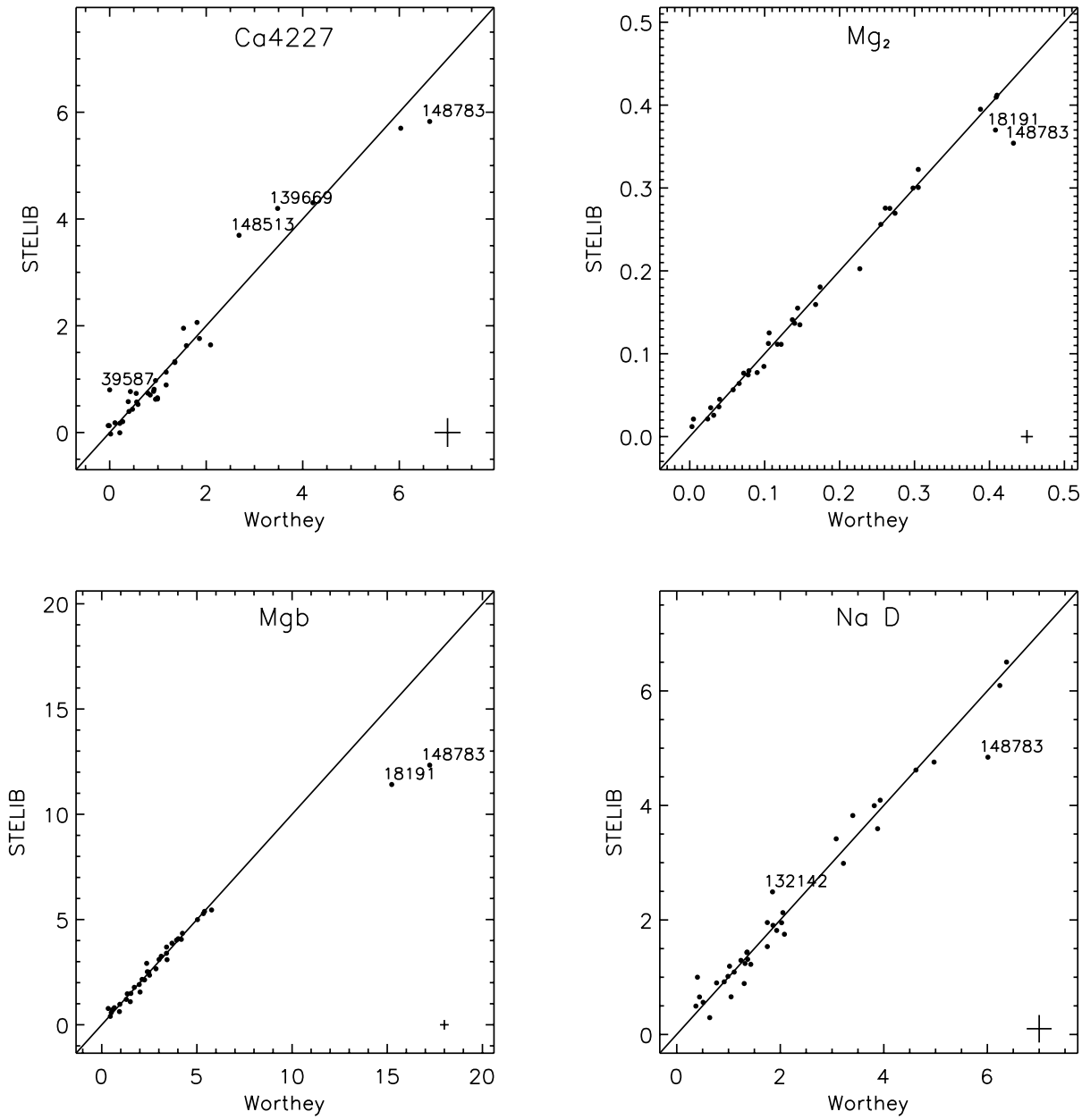

FIG. 2.—Comparison of the calibrated indices of the STELIB library with the corresponding Worthey catalog indices. Outliers are indicated by their HD number, and observational errors are indicated by crosses in each panel.

knew the stellar $T_{\rm eff}$, $\log g$, [Fe/H], and microturbulence values. Unfortunately, the uncertainties on the actual stellar parameter values can lead to contradictory results. In fact, by using different combinations of $T_{\rm eff}$, $\log g$, and [Fe/H] it is possible to reproduce the strength of the observed features with synthetic spectra computed by using different [α/Fe] values. As an example, Figure 5 shows that the observed Mg features in the STELIB spectrum of HD 77729 can be reproduced in an almost equivalent way by both NSSA and SSA synthetic spectra by varying the values of $T_{\rm eff}$, $\log g$, and [Fe/H] within their uncertainties. In this particular case we used as a starting point (Fig. 5*a*) the values $T_{\rm eff} = 4271$, $\log g = 2.0$, and [Fe/H] $= -0.40$ as given by Gratton & Ortolani (1984) and reported by Le Borgne et al. (2003), which are affected by uncertainties of ± 150 K, ± 0.5 dex, and ± 0.2 dex, respectively. A good reduction of the discrepancy between the observed and the synthetic spectrum can be achieved by assuming either an α-enhancement (Fig. 5*b*) or a lower temperature (Fig. 5*c*) or a higher [Fe/H] (Fig. 5*d*). It is clear that to discriminate between NSSA and SSA cases we must rely on a method not requiring an exact knowledge of $T_{\rm eff}$, $\log g$, and [Fe/H]. Therefore, in § 4.1 we use the method described in Paper I, which completely fulfills the above requirement. Only in a few cases (see § 4.2) do we take advantage of the knowledge of [Fe/H] from TAYCAT to increase the sensitivity of our method.

4.1. *Detection Independent of Atmosphere Parameter Knowledge*

In order to identify the α-enhanced candidates in our sample, we applied the technique fully described in Paper I. The sensitivity of the index-index diagrams NaD versus Ca4227, NaD versus Mg_2, NaD versus Mg *b*, and NaD versus CaMg= (A×Ca4227+Mg_2) to α-enhancement found in Paper I for [Fe/H] ≥ -1.0 has also been confirmed at [Fe/H] $= -1.5$.

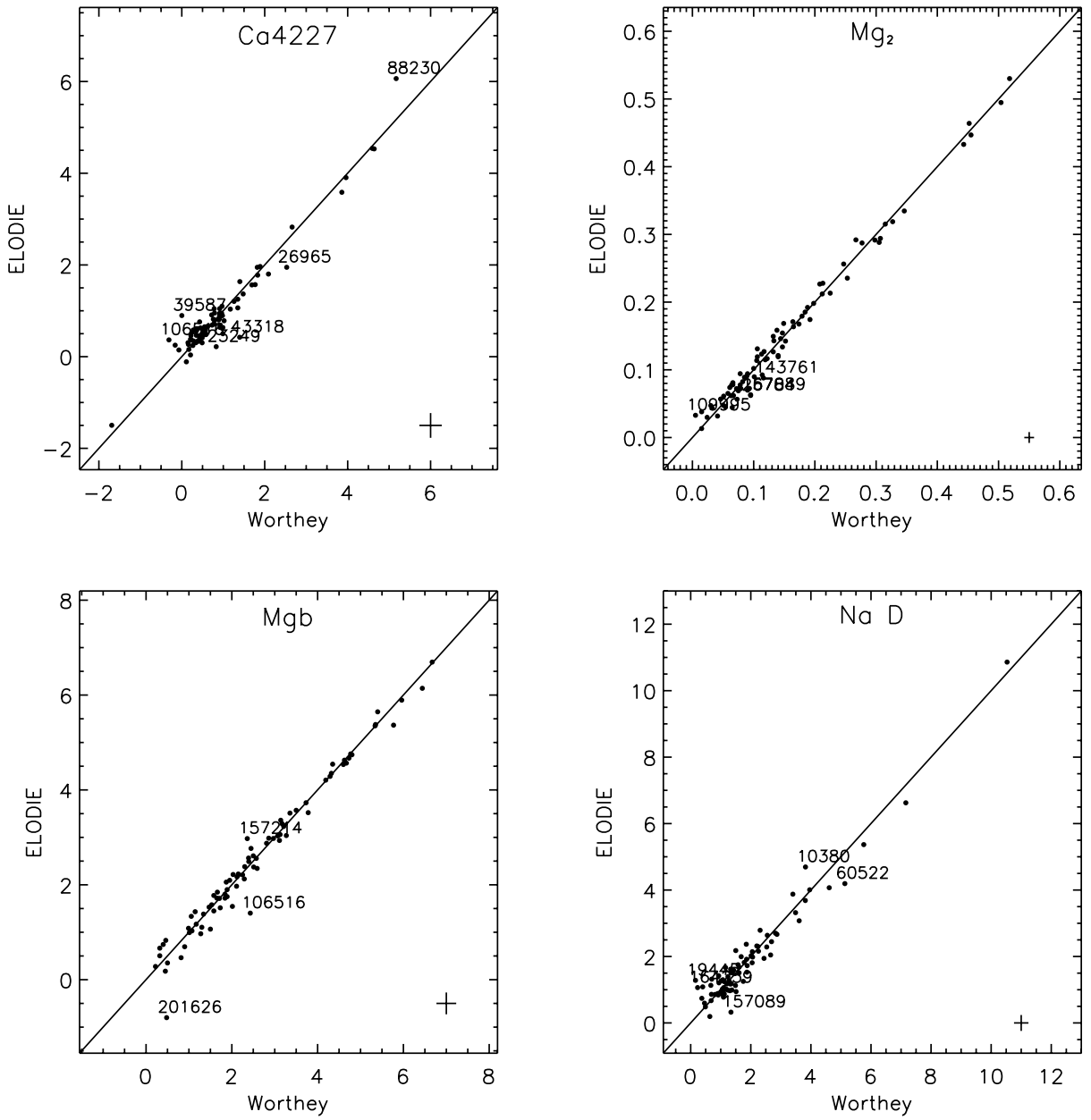

FIG. 3.—Comparison of the calibrated indices of the ELODIE archive with the corresponding Worthey catalog indices. Outliers are indicated by their HD number, and observational errors are indicated by crosses in each panel.

Furthermore, the same boundary lines depicted in Figure 8 of Paper I can be used.

We recall that only stars that fall below these lines at a distance higher than the observational errors are considered bona fide candidates. As in Paper I, distances are defined as $d = [(\Delta_1/\epsilon_1)^2 + (\Delta_2/\epsilon_2)^2]^{1/2}$, where Δ_1, Δ_2 and ϵ_1, ϵ_2 are the X and Y differences between the boundary line and the star position and the observational errors of the two indices in each diagram, respectively. As detection threshold in d the value $\sqrt{2}$ is assumed.

We can try to identify, but with a lower confidence, SSA stars by picking up those well above the boundary lines in the NaD versus Ca4227, NaD versus Mg_2, and NaD versus CaMg diagrams.[4] It is worth noting that we cannot exclude the presence of α- or mildly α-enhanced stars above the boundary lines. We recall, in particular, the problem of a possible contamination of the observed NaD index value by interstellar absorption for the more distant stars. In such a case, NaD interstellar absorption contribution can move an α-enhanced star quite above the boundary line.

TABLE 1
THE DISTRIBUTION OF TAYCAT STARS IN THE FOUR OBSERVATIONAL DATA SETS

Data Set	Worthey	Cananea	STELIB	ELODIE
Worthey.....	168			
Cananea.....	42	135		
STELIB.....	27	30	73	
ELODIE.....	62	38	26	195

[4] The NaD vs. Mg b diagram is not suitable to this purpose as can be seen in Fig. 7c of Paper I.

TABLE 2
DETECTION OF α-ENHANCED CANDIDATE STARS

HD (1)	Spectral Type (2)	[Fe/H] (3)	Error (4)	Code (5)	Cananea (6)	STELIB (7)	ELODIE (8)	Worthey (9)	Results (10)
6.....	G9 III:	0.079	0.101	g	N??N	...	...	...	?
693.....	F5 V	−0.419	0.043	d	...	...	NN?N	...	S
1461.....	G0 V	0.131	0.077	d	...	...	NN?N	NN?N	S

NOTE.—Table 2 is published in its entirety in the electronic edition of the *Astrophysical Journal*. A portion is shown here for guidance regarding its form and content.

Table 2 summarizes the results of this detection approach applied to the stars in the four observational data sets described in § 2.1. For each star identified by its HD number, we list in columns (2)–(5) the spectral classification from SIMBAD, [Fe/H], its error, and a code to distinguish between dwarfs (d) and giants (g) from TAYCAT. In the following four-character wide columns we indicate the presence of the star in each data set and its classification with respect to α-enhancement in each of the four index-index diagrams. The capital letter "Y" is used for bona fide α-enhanced candidates, and the capital letter "N" is used for SSA candidates. The stars marked with "////" are too cool to be compared with our SSA and NSSA grids; their low temperatures are inferred from the position of the observed points in the diagrams and confirmed by looking at data in Taylor (2003a) and by using temperature estimates from broadband photometry. Column (10) of Table 2 lists the code indicating the classification of the star with respect to α-enhancement (see § 4.3).

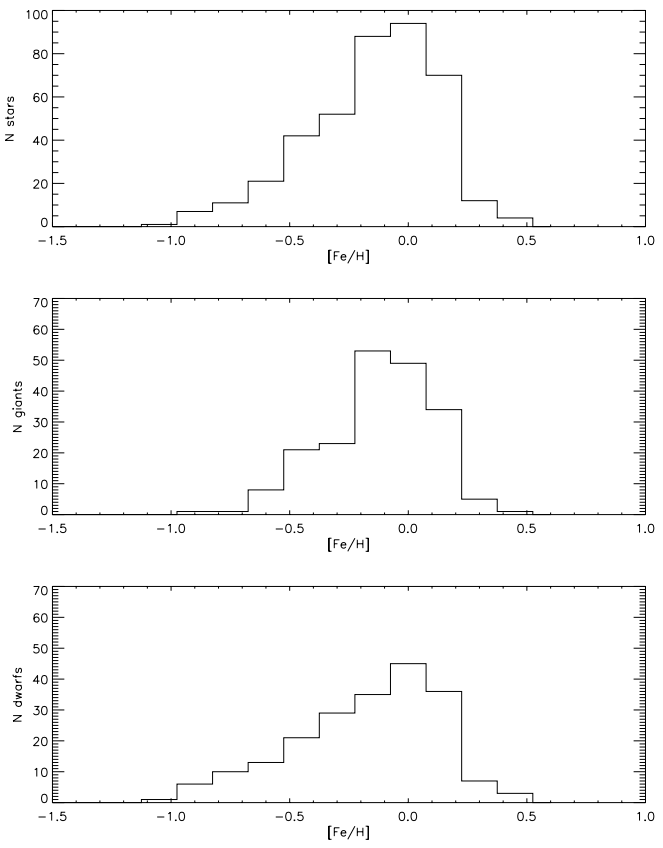

FIG. 4.—[Fe/H] histograms of the total sample and of giants and dwarfs, separately.

4.2. *Detection Based on* [Fe/H] *Knowledge*

We recall that the boundary lines used to discriminate between NSSA and SSA stars were drawn by using synthetic indices spanning all the theoretical grid [Fe/H] values (see Fig. 7 of Paper I). Several times, the observed points in the index-index diagrams fall at a distance from the boundaries lower than the adopted threshold. In these cases, we decided to take advantage of the knowledge of the individual [Fe/H] value to derive for each star an ad hoc boundary line based on the SSA and NSSA loci of synthetic indices computed in a restricted interval of [Fe/H]. To be conservative, we assumed a range of ± 0.5 dex, which is as high as twice the highest uncertainty given in TAYCAT, around the stellar [Fe/H] value. Then we checked the observed point position with respect to its ad hoc boundary line. The classification results obtained, which are

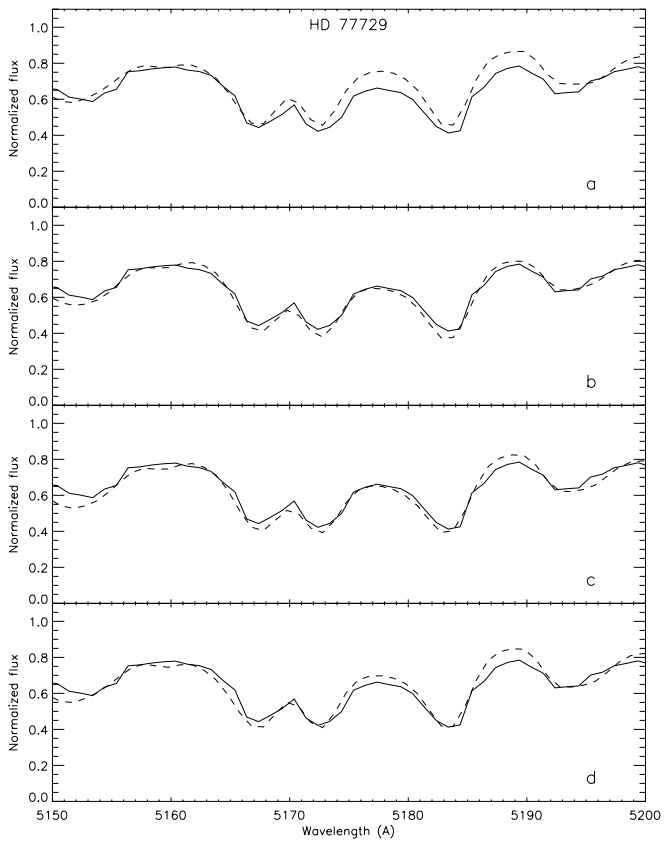

FIG. 5.—HD 77729. Comparison of observed STELIB spectrum (*solid line*) and synthetic ones (*dashed lines*). (*a*) SSA synthetic spectrum computed with $T_{\rm eff} = 4271$ K, $\log g = 2.0$, and [Fe/H] $= -0.40$ (Gratton & Ortolani, 1984); (*b*) NSSA synthetic spectrum computed with $T_{\rm eff} = 4271$ K, $\log g = 2.0$, [Fe/H] $= -0.40$, and $[\alpha/{\rm Fe}] = 0.40$; (*c*) SSA synthetic spectrum computed with $T_{\rm eff} = 4146$ K, $\log g = 2.0$, and [Fe/H] $= -0.40$; (*d*) SSA synthetic spectrum computed with $T_{\rm eff} = 4271$ K, $\log g = 2.0$, and [Fe/H] $= -0.15$.

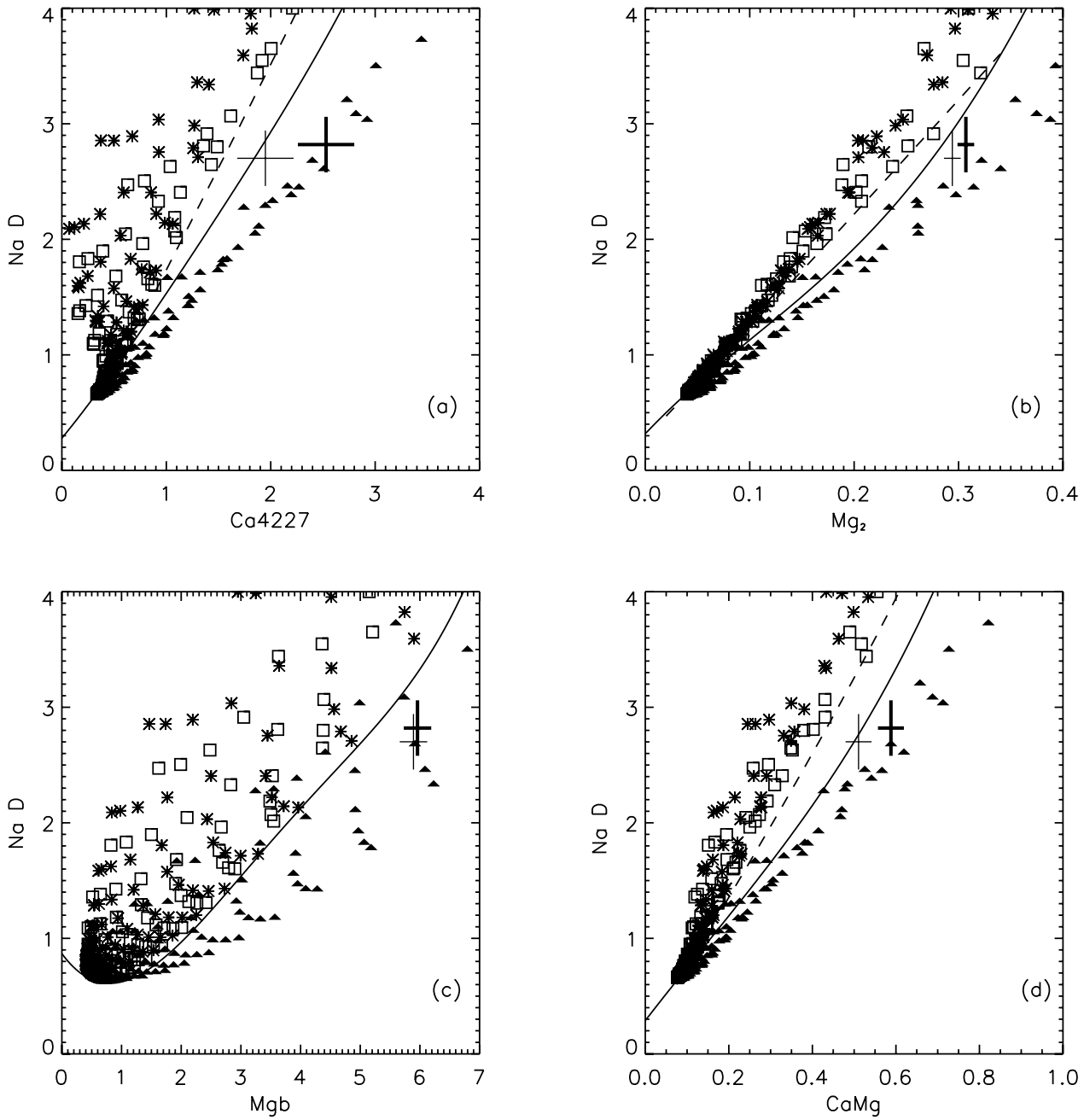

FIG. 6.—Example of detection based on [Fe/H] knowledge: HD 26965. Observed Lick indices from ELODIE archive (*thin plus sign*) and Worthey catalog (*thick plus sign*) are plotted together with the standard boundary lines (*solid line*), the ad hoc boundary lines (*dashed line*); in this particular case the standard and the ad hoc boundary lines in panel *c* coincide. Symbols indicate the SSA grid points at [Fe/H] = 0.00 (*asterisks*), and at [Fe/H] = −0.50 (*open squares*), and NSSA grid points at [Fe/H] = −0.50 (*filled triangles*).

dependent on the assumed [Fe/H] values, are indicated with "Y" or "N" in Table 2; if no clear indication is achievable, a question mark is given. As an example, Figure 6 shows the case of HD 26965, [Fe/H] = −0.295. The ELODIE and Worthey observed points do not fall at a distance below the "standard" boundary lines (*solid line*) greater than the adopted threshold in Figures 6*a*, 6*b*, 6*d*, and 6*b*, respectively. This condition is fulfilled in all the panels if we measure the distance from the ad hoc boundary lines (*dashed line*) drawn by looking only at the SSA points at [Fe/H] = 0.00 and [Fe/H] = −0.50.

4.3. *Final Classification*

By cross-checking the stars belonging to more than one data set, we found only two of them (HD 43318 and HD 198149) with discrepant classification, i.e., with a Y or a y for one data set and with an "N" or "n" in another data set for the same diagram. Looking at all the common data sets does not contradict the classification of any of the other 122 stars; i.e., any Y, y, N, and n in one data set is matched by either the same letter or by a "?" in the other data set(s). As far as HD 43318 and HD 198149 are concerned, in both cases the contradiction is between the results of the fourth index-index diagram, i.e., NaD versus CaMg, since the ELODIE data indicate an SSA nature while the Worthey data are in favor of an α-enhancement. Actually, the $CaMg_E$ and $CaMg_W$ values for HD 43318 and the NaD_E and NaD_W for HD 198149 differ more than expected, leading to a contradictory classification. It is very likely that in both cases the discrepancy can be attributed to observational

problems. The agreement in all the other 122 cases shows that, apart from the two "anomalous" cases HD 43318 and HD 198149 discussed above, there is a good consistency among the indices computed from the four different data sets, thus confirming the validity of the adopted transformations from instrumental to Lick/IDS system.

The combined results after analyzing all four diagrams for each of the four data sets are given in columns (6)–(9) of Table 2. We found a total number of 162 α-enhancement indications, corresponding to 60 individual stars, which are marked by a letter A in column (10). We classified as α-enhanced stars all those with at least one Y or y. As far as the detection or not in the different diagrams is concerned, we recall that stars characterized by [Ca/Fe] enhancement are more likely to be detected in the first index-index diagram, while those showing [Mg/Fe] enhancement tend to be detected in the second and in the third ones. The fourth diagram provides an indication of the average [α/Fe] enhancement.

As far as the SSA stars are concerned, we considered only three diagrams in each data set, excluding the NaD versus Mg *b* one, leading to 146 individual stars indicated by a letter S in column (10). A star to be classified SSA must have the letter N or n in all three effective diagrams.

In conclusion, we are able to classify about one-half of the total sample. The failure to determine the SSA or NSSA nature of the remaining half is most probably due to the following causes: (1) the unavoidable loss of sensitivity of our method at high temperatures due to the coalescence and vanishing of the observed and synthetic indices, and (2) our choice of the $\sqrt{2}$ threshold in the dimensionless distance measured between the observed point and the discrimination boundary. In the future, the availability of observed indices with much higher accuracy than the present one would permit us to significantly reduce the uncertainty areas around the boundary lines.

5. α-ENHANCEMENT VERSUS [Fe/H] AND KINEMATICAL PROPERTIES

In the following, in order to soundly compare the properties of the α-enhanced and of the SSA groups, we restricted our analysis to the stars with an NaD index large enough to avoid the problem of misclassification as a result of contamination by interstellar absorption. By adopting by rule of thumb 0.65 Å as the minimum acceptable value of NaD, we reduced the number of identified α-enhanced and SSA stars to 54 and 137, respectively.[5] The upper panel of Figure 7 shows the [Fe/H] distribution of the remaining 191 stars; the lower panel displays the percentage distribution of α-enhanced and SSA stars in each [Fe/H] = 0.15 dex bin. It is evident that in going from high to low [Fe/H] values the percentage of SSA stars decreases until it vanishes at [Fe/H] = −0.50. On the other hand, the percentage of α-enhanced stars decreases toward high [Fe/H] values and vanishes at [Fe/H] ≥ +0.20. No significant difference was found by looking at dwarfs and giants separately. Our results confirm the increasing importance of the α-enhancement phenomenon at low [Fe/H] but show also the presence of both α-enhanced and SSA stars in the range $-0.50 \leq [\mathrm{Fe/H}] \leq +0.20$.

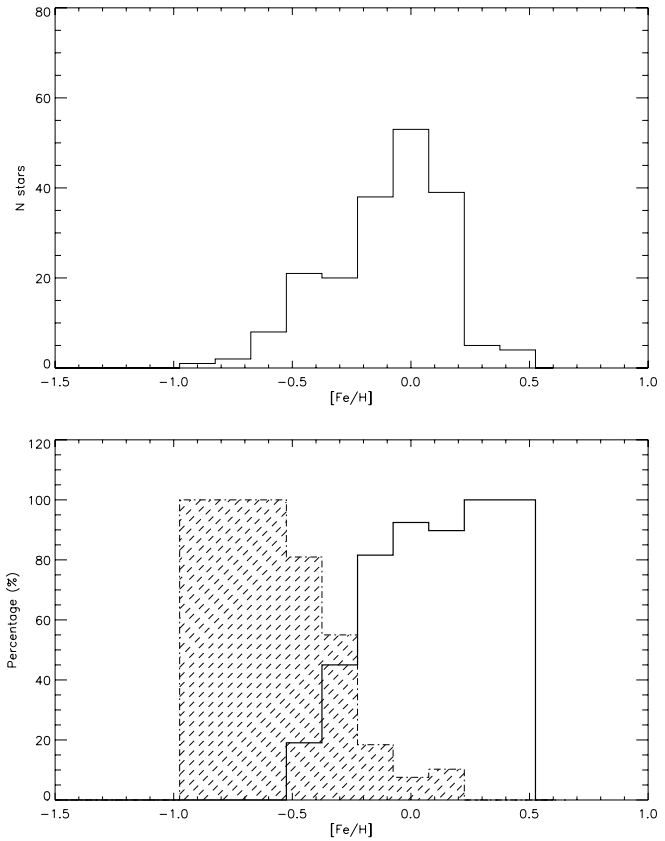

FIG. 7.—[Fe/H] histogram of the restricted sample of 191 stars discussed in § 5 (*upper panel*) and percentage distributions (*lower panel*) of α-enhanced (*dashed area*) and SSA (*empty area*) stars.

In order to investigate whether the α-enhanced and SSA stars belong or not to the same Galactic component, we computed their Galactic velocity components starting from radial velocities, proper motions, and parallaxes from SIMBAD. We derived the (U_{LSR}, V_{LSR}, W_{LSR}) values of 51 and 124 α-enhanced and SSA stars, respectively. Table 3 compares the mean values and the standard deviations of the Galactic velocity of the SSA and of the α-enhanced groups with the characteristic values of the Galactic thin and thick disks by

[5] We removed from the SSA group also HD 6833: being a quite distant star at low galactic latitude its NaD index is very likely to be heavily contaminated by interstellar absorption.

TABLE 3

KINEMATICAL PROPERTIES OF α-ENHANCED AND SSA STARS

Group	$\langle U_{\mathrm{LSR}} \rangle$ (km s^{-1})	$\langle V_{\mathrm{LSR}} \rangle$ (km s^{-1})	$\langle \lvert W_{\mathrm{LSR}} \rvert \rangle$ (km s^{-1})	σ_U (km s^{-1})	σ_V (km s^{-1})	σ_W (km s^{-1})
SSA	5 ± 3	−6 ± 2	9 ± 1	31 ± 3	20 ± 2	12 ± 1
α	7 ± 9	−30 ± 6	26 ± 3	66 ± 8	44 ± 7	33 ± 4
Thin disk[a]	...	0 ± 2	...	39 ± 2	20 ± 2	20 ± 1
Thick disk[a]	...	−39 ± 5	...	63 ± 6	39 ± 4	39 ± 4

[a] Soubiran et al. (2003).

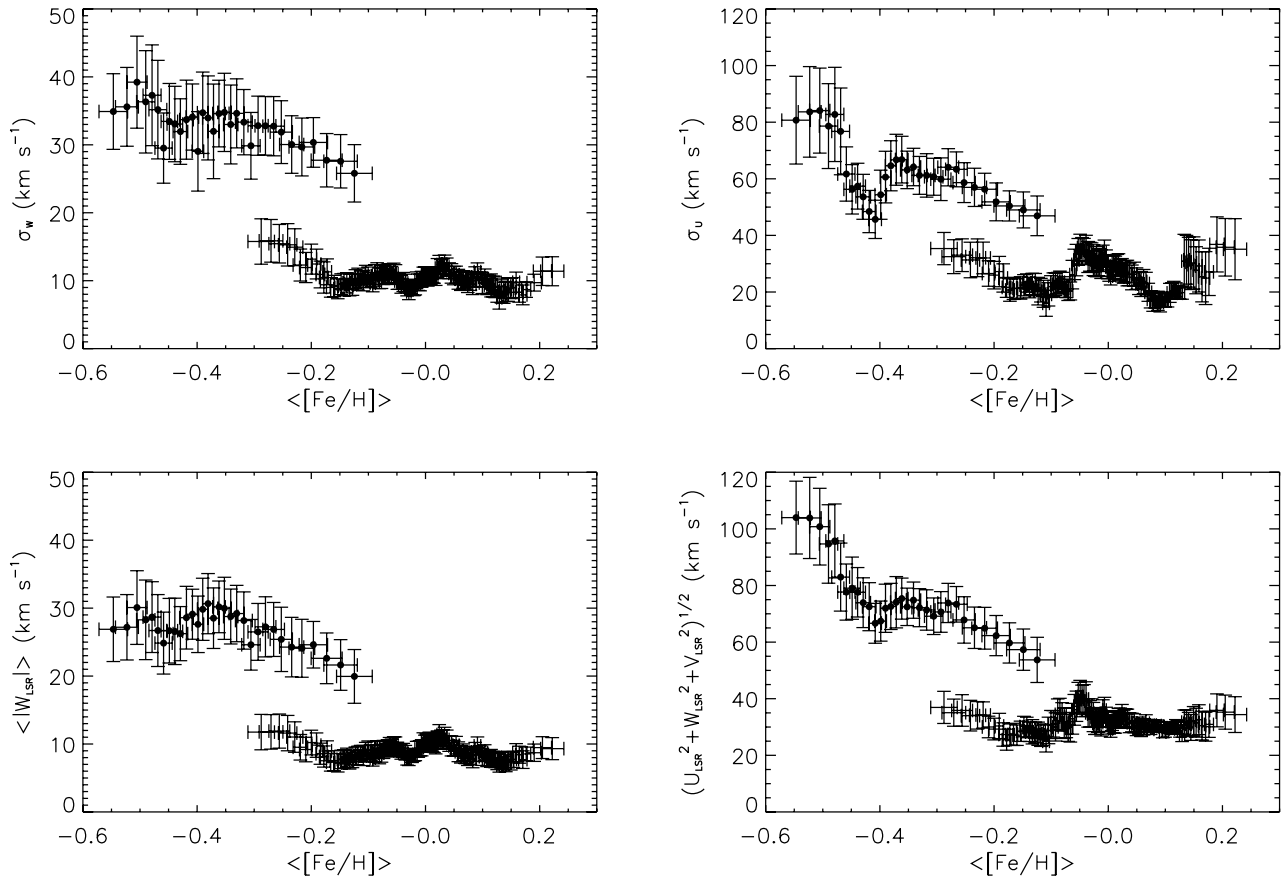

FIG. 8.—Kinematical properties vs. [Fe/H] of α-enhanced (*filled circles*) and SSA stars with bootstrap error bars (running average 19 points window).

Soubiran et al. (2003). The $\langle V \rangle$ values for the Galactic thin and thick disks have been reduced to the local standard of rest by assuming $V_{\odot} = 12.0$ km s^{-1}.

The errors on the kinematics of the SSA and α-enhanced groups were computed via a bootstrap technique. Bootstrapping was introduced by Efron (1979); it is a computer-based method for estimating the standard error of an estimator. A useful outline of the method can be found in the lectures of the course "Re-sampling techniques for statistical modeling" by G. Bontempi[6] and in an annotated bibliography for bootstrap resampling compiled by R. A. Stine.[7] In our particular case we used the *bbootstrap.pro* IDL routine from the Freudenreich AstroContrib Library.[8]

The similarity in kinematical properties between the α-enhanced group and the Galactic thick disk is evident. This is in agreement with the discussion in Nissen (2004), and it is worth noting that it is obtained from a sample of stars that were not selected according to their Galactic velocities and, therefore, free from any kinematical bias. On the other hand the SSA group kinematics resembles those of the Galactic thin disk. The main difference lies in the low value of the σ_W of the SSA stars. This discrepancy is confirmed by using other estimates of σ_W of the Galactic thin disk, such as those by Gómez et al. (1997) and by Bensby et al. 2003), who found $\sigma_W \lesssim 15/17$ km s^{-1} and $\sigma_W = 16$ km s^{-1}, respectively. On the other hand, Allende Prieto et al. (2004) found $\sigma_W = 13$ km s^{-1} by analyzing solar neighborhood stars within 15 pc and claim that their sample of stars "is representative, kinematically and chemically, of a much larger volume of the local thin disk." Thus, a possible explanation is a selection effect, since the Soubiran et al. (2003) Galactic thin disk sample is mainly constituted by clump giants spanning typically distances from 200 to 800 pc to the Galactic midplane, while our SSA sample contains solar neighborhood stars with a maximum distance of 250 pc to the Sun. On the other hand, it is also possible that the low σ_W of our SSA sample indicates a population of quite young thin disk stars with a quite small dispersion in age (see Fig. 2 by Gómez et al. (1997) for the trend of σ_W vs. age).

As noted above, there is a region of [Fe/H] values in which both α-enhanced and SSA stars can be found. In an attempt to better understand this behavior, we analyzed the trend of the kinematical properties of our stars versus [Fe/H]. Figure 8 shows that the α-enhanced and SSA stars are also well separated in the common [Fe/H] region, indicating their belonging to two different Galactic components. In fact, the values of $\langle |W_{\rm LSR}| \rangle$, $\langle V_{\rm pec} \rangle = \langle (U^2_{\rm LSR} + W^2_{\rm LSR} + V^2_{\rm LSR})^{1/2} \rangle$, σ_W, and σ_U of α-enhanced stars, computed using a running average, are always larger than the corresponding values of SSA stars at the same [Fe/H]. These results confirm once more that the apparent degeneracy of α-enhanced and SSA stars at $-0.50 \leq$[Fe/H]$\leq +0.20$ can be removed by looking at the stellar kinematics and can be attributed to an overlap in metallicity of two galactic components. Figure 8 indicates a threshold between the two components at about $\langle V_{\rm pec} \rangle = 50$ km s^{-1}. This value casts some doubts on the straightforward identification

[6] See http://www.ulb.ac.be/di/map/gbonte/Stat104.html.
[7] See http://www-stat.wharton.upenn.edu/%7Ebob/mich/bibliography.pdf.
[8] See http://www.astro.washington.edu/deutsch/idl/htmlhelp/slibrary14.html.

of the α-enhanced and SSA star galactic components with the thick and thin disks, as suggested by the data in Table 3. In fact, several authors (see, e.g., Nissen 2004) adopt a much higher threshold value, $\langle V_{\rm pec} \rangle = 85$ km s^{-1} to separate thick and thin disk stars.

6. CONCLUSIONS

Computed Lick indices for 402 mildly metal-poor, solar, and supersolar stars, i.e., with [Fe/H] in the range -1.0 to 0.5 dex, are compared with predictions from solar, solar-scaled, and α-enhanced synthetic spectra. The application of the selection method presented in Paper I provided a list of 60 bona fide α-enhanced stars and of 146 SSA stars.

The analysis of the kinematical properties of the two samples showed that α-enhanced and SSA stars very likely belong to two different Galactic components. The α-enhanced and SSA star group kinematics and their behavior versus [Fe/H] values show strong similarities with those of the thick and thin disks, respectively, even if the presence of some quantitative discrepancy in the σ_W values cannot be ruled out.

The results presented here suggest that a comparison of the α-enhanced and SSA group properties with the results of detailed analysis of the Galactic thin and thick disks, based on their subdivision in several components according to various distances to the Galactic plane and/or ages, would be very fruitful. Unfortunately, analyses like those, for example, by Soubiran et al. (2003) require a number of stars much larger than that available at present to reach a sound statistical evidence. Thus, we have already started an observing program at the G. Haro Observatory, Cananea, Mexico, which should allow us to better characterize α-enhanced and SSA Galactic components and to increase the statistical validity of the results presented in this paper.

This work received partial financial support from the Mexican CONACyT via grant 36547-E, from Università degli Studi di Trieste (60% grants) and from MIUR COFIN-2003028039.

REFERENCES

Allende Prieto, C., Barklem, P. S., Lambert, D. L., & Cunha, K. 2004, A&A, 420, 183
Baranne, A., et al. 1996, A&AS, 119, 373
Bensby, T., Feltzing, S., & Lundström, I. 2003, A&A, 410, 527
Cayrel de Strobel, G., Soubiran, C., & Ralite, N. 2001, A&A, 373, 159
Chen, Y. Q., Zhao, G., Nissen, P. E., Bai, G. S., & Qiu, H. M. 2003, ApJ, 591, 925
Efron, B. 1979, Ann. Stat., 7, 1
Franchini, M., Di Marcantonio, P., Morossi, C., Malagnini, M. L., Chavez, M., & Rodríguez, L. 2004, ApJ, 601, 485 (Paper I)
Gómez, A. E., Grenier, S., Udry, S., Haywood, M., Meillon, L., Sabas, V., Sellier, A., & Morin, D. 1997, in *Hipparcos*, Venice '97, ed. B. Battrick, M. A. C. Perryman, & P. L. Bernacca (ESA SP-402; Noordwijk: ESA), 621
Gratton, R. G., & Ortolani, S. 1984, A&A, 137, 6
Gray, R. O., & Corbally, C. J. 1994, AJ, 107, 742
Grevesse, N., & Sauval, A. J. 1998, Space Sci. Rev., 85, 161
Le Borgne, J. F., et al. 2003, A&A, 402, 433
Morossi, C., Di Marcantonio, P., Franchini, M., Malagnini, M. L., & Chavez, M. 2002, ApJ, 577, 377
Nissen, P. E. 2004, in Origin and Evolution of the Elements, ed. A. McWilliam & M. Rauch (Cambridge: Cambridge Univ. Press), 156
Norris, J. E. 1999, Ap&SS, 265, 213
Soubiran, C. Bienaymé, O., & Siebert, A. 2003, A&A, 398, 141
Taylor, B. J. 1999, A&AS, 134, 523
———. 2003a, A&A, 398, 721
———. 2003b, A&A, 398, 731
Worthey, G., Faber, S. M., Gonzalez, J. J., & Burstein, D. 1994, ApJS, 94, 687